arXiv:hep-ph/9706334v2 19 Jan 1998

FSU-HEP-970527
DESY 97-111

Charm quark and $D^{*\pm}$ cross sections in deeply inelastic scattering at HERA

B. W. Harris
Physics Department
Florida State University
Tallahassee, Florida 32306-4250, USA

J. Smith*
DESY
Notkestrasse 85
D-22603 Hamburg, Germany
(May 1997)

Abstract

A next-to-leading order Monte Carlo program for the calculation of heavy quark cross sections in deeply inelastic scattering is described. Concentrating on charm quark and $D^{*\pm}(2010)$ production at HERA, several distributions are presented and their variation with respect to charm quark mass, parton distribution set, and renormalization/factorization scale is studied.

PACS number(s): 12.38.Bx,13.60.Hb,14.65.Dw

Typeset using REVTEX

*On leave from ITP, SUNY at Stony Brook, Stony Brook, NY 11794-3840, USA

I. INTRODUCTION

Electromagnetic interactions have long been used to study both hadronic structure and strong interaction dynamics. Examples include deeply inelastic lepton-nucleon scattering, hadroproduction of lepton pairs, the production of photons with large transverse momenta, and various photoproduction processes involving scattering of real or very low mass virtual photons from hadrons. In particular, heavy quark production in deeply inelastic electron-proton scattering (DIS) is calculable in QCD and provides information on the gluonic content of the proton which is complementary to that obtained in direct photon production or structure function scaling violations. In addition, it forces one to address such issues as when the mass of the heavy quark should be neglected, and how this is done consistently.

Activity in the area of neutral current DIS charm quark production has increased recently with new data becoming available from ZEUS [1] and H1 [2] at HERA. In particular, substantial samples of $D^{*\pm}(2010)$ hadrons have been obtained. On the theoretical side, much attention has been given to the study of heavy quark contributions to the proton structure function. They have been calculated to next-to-leading order in fully inclusive [3], single inclusive [4], and fully differential (exclusive) [5] forms as QCD corrections to the photon-gluon fusion process (i.e. in $\mathcal{O}(\alpha_s^2) + \mathcal{O}(\alpha_s^3)$ using three flavor parton densities). Experimentally [1,2,6] and phenomenologically [7,8], it is this process that is seen to dominate near the threshold region. However, well above threshold the heavy quark may be considered massless and included in the parton distribution function of the proton. Various schemes to match these two regions have been proposed [9–11]. Despite all of the attention structure functions have received, much less has been done to explore the actual heavy quark differential cross sections in DIS which are, in fact, much easier to measure experimentally.

The purpose of this work is to present next-to-leading order cross sections for charm quark production in the x and Q^2 region covered by the HERA collider. Additionally, predictions for heavy hadrons, namely $D^{*\pm}(2010)$, are given. The calculation is implemented in a Monte Carlo style program which allows the simultaneous histogramming of many distributions incorporating experimental cuts. It represents an elaboration of the brief results already presented by one of us [12], and an application of the fully differential heavy quark structure functions calculated in [5]. No experimental data is shown here because the results have already been added to several of the plots in [1] (see also [12]). An extensive comparison will be given elsewhere. Herein, the calculation itself is discussed and the variation with respect to the theoretical parameters is studied. Heavy quark correlations have also been calculated for hadroproduction [13], photoproduction [14], and photon-photon collisions [15,16] allowing for the possiblility of an extensive comparison with experimental data.

The calculation was performed using the subtraction method which is based on the replacement of divergent (soft or collinear) terms in the squared matrix elements by generalized distributions. The method was first used in the context of electron-positron annihilation [17] and its essence is described and compared to the phase-space slicing method [18] in the introduction of a paper by Kunszt and Soper [19].

The remainder of the paper is as follows. A review of the subtraction method and other aspects of the calculation, including how the hadronization is modeled, are given in Sec. II. Numerical results and a discussion of related physics issues are presented in Sec. III. The conclusions are given in Sec. IV.

II. CALCULATION

In this section the calculation of the charm quark cross section in deeply inelastic scattering is described. First, the cross section is written in terms of the charm quark contribution to the proton structure functions. Then the next-to-leading order QCD corrections to the structure functions are reviewed. Finally we describe the connection with the production of heavy hadrons containing a charm quark.

A. Cross section in terms of structure functions

The reaction under consideration is charm quark production *via* neutral-current electron-proton scattering.

$$e^-(l) + P(p) \to e^-(l') + Q(p_1) + X\,. \tag{2.1}$$

When the momentum transfer squared $Q^2 = -q^2 > 0$ ($q = l - l'$) is not too large $Q^2 \ll M_Z^2$, the contribution from Z boson exchange is kinematically suppressed and the process is dominated by virtual-photon exchange. The cross section may then be written in terms of structure functions $F_2^c(x, Q^2, m)$ and $F_L^c(x, Q^2, m)$ which depend explicitly on the charm quark mass m_c [3,20] as follows:

$$\frac{d^2\sigma}{dydQ^2} = \frac{2\pi\alpha^2}{yQ^4}\left\{\left[1 + (1-y)^2\right] F_2^c(x, Q^2, m_c) - y^2 F_L^c(x, Q^2, m_c)\right\} \tag{2.2}$$

where $x = Q^2/2p\cdot q$ and $y = p\cdot q/p\cdot l$ are the usual Bjorken scaling variables and α is the electromagnetic coupling. The scaling variables are related to the square of the c.m. energy of the electron-proton system $S = (l+p)^2$ *via* $xyS = Q^2$. The total cross section [20] is given by

$$\sigma = \int_{4m_c^2/S}^{1} dy \int_{m_e^2 y^2/(1-y)}^{yS-4m_c^2} dQ^2 \left(\frac{d^2\sigma}{dydQ^2}\right) \tag{2.3}$$

where m_e is the electron mass. In deriving Eq. (2.2), one integrates over the azimuthal angle between the plane containing the incoming and outgoing electrons and the plane containing the incoming proton and the outgoing charm quark.

As mentioned in the introduction, this process is described near threshold in the framework of perturbative QCD by flavour creation through the virtual-photon-gluon fusion process

$$\gamma^*(q) + g(k_1) \to Q(p_1) + \bar{Q}(p_2). \tag{2.4}$$

The structure functions follow [3,5] from the longitudinal σ_L and transverse σ_T cross sections for this reaction *via* $F_2^c = (Q^2/4\pi^2\alpha)\,(\sigma_L + \sigma_T)$ and $F_L^c = (Q^2/4\pi^2\alpha)\,\sigma_L$. Thus, QCD corrections to the reaction (2.1) correspond to QCD corrections to (2.4) to which we now turn. The supersript c will henceforth be dropped to simplify notation.

B. QCD corrections to the heavy quark structure functions

Within the context of perturbative QCD, structure functions are expressed as a product of the running coupling, the parton densities, and the hard scattering cross sections. The result is a physical quantity, but the individual terms can be defined in a convenient scheme which moves terms from one factor to another. All schemes should give the same result for the product, up to terms of higher order.

A next-to-leading order calculation of the heavy quark contributions to the proton structure functions requires the one-loop virtual corrections to (2.4). For this set of diagrams, the renormalization was carried out so that divergences coming from the light quarks were subtracted in the standard $\overline{\rm MS}$ scheme, while the divergences coming from heavy quark loops were subtracted at zero external momenta. This is the scheme originally proposed in [21] in which the mass m only appears in the hard scattering cross sections. As a consequence, below the subtraction scale, only the number of (massless) light flavours appears in the running coupling and in the splitting functions used in the parton evolution equations. At the subtraction scale $\mu = m$ there are matching conditions for both the running coupling and the light flavour densities [21]. Therefore, to order α_s, there is no charm density at the scale $\mu = m$ [21], [22].

Consequently, one should use only parton distribution sets that were derived from data using the same renormalization scheme. Examples of such densities are GRV94 [23] and CTEQ4F3 [24]. At larger scales there is a charm density proportional to $\alpha_s \ln(\mu^2/m_c^2)$, which grows at the expense of a reduction in the gluon density. One of the interesting problems in the analysis of charm quark contributions to deeply inelastic scattering is to understand the transition region from the photon-gluon predictions based on three light flavours to a charm density picture with four light flavours. The matching conditions become more complicated as one goes to higher order. The corresponding two-loop matching conditions for the flavour densities have been calculated in [11] wherein they were found to have finite terms at $\mu = m$.

In addition to the virtual corrections described above, there is also a contribution from the gluon-bremsstrahlung process

$$\gamma^*(q) + g(k_1) \to Q(p_1) + \bar{Q}(p_2) + g(k_2) \tag{2.5}$$

and new production mechanisms not present at leading order, which are given by

$$\begin{aligned} \gamma^*(q) + q(k_1) &\to Q(p_1) + \bar{Q}(p_2) + q(k_2) \\ \gamma^*(q) + \bar{q}(k_1) &\to Q(p_1) + \bar{Q}(p_2) + \bar{q}(k_2) \end{aligned} \tag{2.6}$$

where $(\bar{q})q$ is a massless (anti-)quark. The contribution to the structure functions resulting from these processes have been calculated in a fully differential [5] form and are suitable for use in constructing a Monte Carlo style program because one has full access to the final state partonic four vectors.

Briefly, the computation in [5] was carried out using the subtraction method which is based on the replacement of divergent (soft or collinear) terms in the squared matrix elements by generalized plus distributions. This allows one to isolate the soft and collinear poles within the framework of dimensional regularization without calculating all the phase space integrals in a space-time dimension $n \neq 4$ as is required in a traditional single particle

inclusive computation. In this method the expressions for the squared matrix elements in the collinear limit appear in a factorized form, where poles in $n-4$ multiply splitting functions and lower order squared matrix elements. The cancellation of collinear singularities is then performed using mass factorization. The expressions for the squared matrix elements in the soft limit also appear in a factorized form where poles in $n-4$ multiply lower order squared matrix elements. The cancellation of soft singularities takes place upon adding the contributions from the renormalized virtual diagrams. Since the final result is in four-dimensional space time, one can compute all relevant phase space integrations using standard Monte Carlo integration techniques.

The resultant (differential) structure functions may be written in the form

$$F_k(x,Q^2,m) = \frac{Q^2\alpha_s(\mu^2)}{4\pi^2 m^2}\int_{\xi_{\min}}^1 \frac{d\xi}{\xi}\left\{\left[c_{k,g}^{(0)} + 4\pi\alpha_s(\mu^2)\left(c_{k,g}^{(1)} + \bar{c}_{k,g}^{(1)}\ln\frac{\mu^2}{m^2}\right)\right]e_H^2 f_{g/P}(\xi,\mu^2)\right.$$
$$\left. + 4\pi\alpha_s(\mu^2)\sum_{i=q,\bar{q}} f_{i/P}(\xi,\mu^2)\left[e_H^2\left(c_{k,i}^{(1)} + \bar{c}_{k,i}^{(1)}\ln\frac{\mu^2}{m^2}\right) + e_i^2\, d_{k,i}^{(1)} + e_i\, e_H\, o_{k,i}^{(1)}\right]\right\} \tag{2.7}$$

$k = 2, L$. The lower boundary on the integration is $\xi_{\min} = x(4m^2+Q^2)/Q^2$. The parton momentum distributions in the proton are denoted by $f_{i/P}(\xi,\mu^2)$. The mass factorization scale μ_f has been set equal to the renormalization scale μ_r and is denoted by μ. All charges are in units of e. Finally, $c_{k,i}^{(0)}$, $c_{k,i}^{(1)}$, $\overline{c}_{k,i}^{(1)}, (i = g,q,\bar{q})$, and $d_{k,i}^{(1)}$, $o_{k,i}^{(1)}, (i = q,\bar{q})$ are scale independent parton coefficient functions. They are functions of ξ, Q^2, and m. In Eq. (2.7) the coefficient functions are distinguished by their origin. The c-coefficent functions originate from processes involving the virtual photon-heavy quark coupling, while the d-coefficient functions arise from processes involving the virtual photon-light quark coupling and the o-coefficent functions are from the interference between these processes.

In addition to the calculation of [5], the functions $c_{k,i}^{(1)}$, $\overline{c}_{k,i}^{(1)}$, and $d_{k,i}^{(1)}$ were calculated in inclusive form in [3], [4] as two-dimensional integrals and computed numerically. In [25] they were numerically tabulated in grids, with a fast interpolation routine, so that the computation of Eq. (2.7) could be included in a global fit, if desired. Finally, in [26] exact analytic formulae were given for the $d_{k,i}^{(1)}$ together with analytic formulae for all the coefficient functions $c_{k,i}^{(0)}$, $c_{k,i}^{(1)}$, $\overline{c}_{k,i}^{(1)}, (i = g,q,\bar{q})$, and $d_{k,i}^{(1)}, (i = q,\bar{q})$ in the limit $Q^2 >> m^2$. The latter results are necessary to consider a variable flavour scheme in which the coefficient functions are incorporated into redefined light parton densities including a charm density [11].

Naturally, properties of the structure functions give insight into the behavior of the cross section. Therefore the more salient features of the next-to-leading order structure functions will now be summarized. The interested reader can find additional details in the original papers [3–5] and, more so, in the recent phenomenological analyses [8,27–29]. For moderate $Q^2 \sim 10\,\mathrm{GeV}^2$ one finds that the charm quark contribution at small $x \sim 10^{-4}$ is approximately 25% of the total structure function (defined as light parton plus heavy quark contributions). In contrast, the contribution from bottom quarks is only a few percent due to charge and phase space suppression. Thus, the charm quark contribution must be retained, but the bottom quark contribution may be neglected in the following. The gluon initiated contributions (2.4) and (2.5) comprise most of the structure function. The

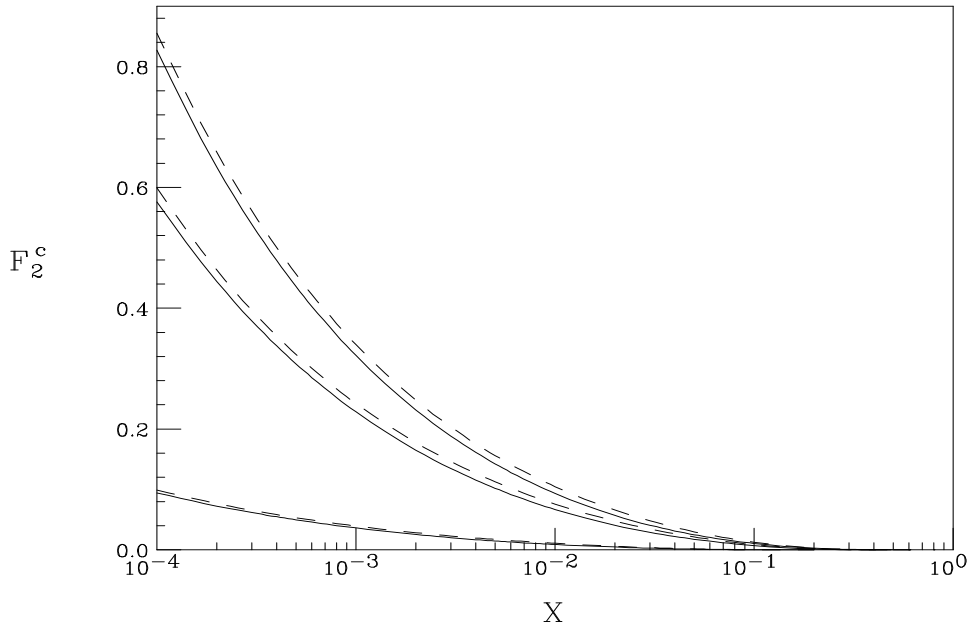

FIG. 1. $F_2^c(x, Q^2, m_c = 1.5\,\mathrm{GeV})$ as a function of x for GRV94 (solid lines) and CTEQ4F3 (dash lines) parton distribution sets for $Q^2 = 3\,\mathrm{GeV}^2$ (bottom), $25\,\mathrm{GeV}^2$ (middle), and $50\,\mathrm{GeV}^2$ (top).

quark initiated processes (2.6) give only a few percent contribution at small x for reasonable scale choices. Results for the charm quark contribution to the proton structure function $F_2^c(x, Q^2, m_c = 1.5\,\mathrm{GeV})$ as a function of x are shown in FIG. 1 for $\mu = \sqrt{Q^2 + 4m_c^2}$ using the GRV94 [23] and CTEQ4F3 [24] parton distribution sets. As mentioned above, these sets were chosen because they have $n_f = 3$ in the evolution and are therefore the most consistent sets to use with the NLO calculation. The curves show a marked rise in the structure function at small x due primarily to the rapidly rising gluon distribution. The renormalization/factorization scale dependence is rather flat, especially at small x where the structure function is largest. This is demonstrated in FIG. 2 for various x and Q^2 values. By far the largest uncertainty in the calculation of the structure functions is the value of the heavy quark mass. For charm production, for example, a $\pm 10\%$ variation of the mass about the central value of $m_c = 1.5\,\mathrm{GeV}$ gives a $\pm 20\%$ variation in the structure function for moderate Q^2.

C. Fragmentation into heavy hadrons

Experimentally, it is heavy hadrons or their decay productions that are observed. Of interest for HERA is $D^{*\pm}(2010)$ production. Herein, the Peterson *et al.* form of the fragmentation function [30] is used to model the nonperturbative hadronization process.

The cross section for D^* production is obtained by convoluting the charm quark cross section (2.3) with the fragmentation function

$$D(z) = \frac{N}{z[1 - 1/z - \epsilon/(1-z)]^2} \tag{2.8}$$

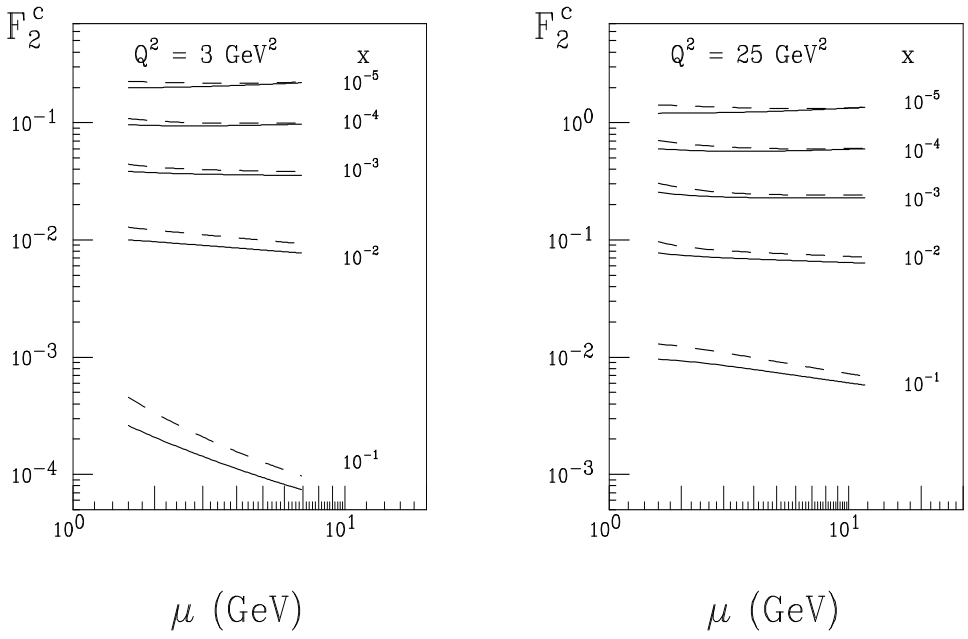

FIG. 2. $F_2^c(x, Q^2, m_c = 1.5\,\mathrm{GeV})$ as a function of the scale μ with $m_c \leq \mu \leq 2\sqrt{Q^2 + 4m_c^2}$ for various x and Q^2 values for the GRV94 (solid lines) and CTEQ4F3 (dash lines) parton distribution sets.

where N is fixed such that $D(z)$ is normalized to unity. The normalization of the cross section is then fixed by the charm quark fragmentation probability $P(c \to D^*) = 0.26$ [31]. The parameter ϵ may be extracted from data [32] and used as input. However, in light of recent work on the subject [33,34], the specific value that should be used in this particular application is not obvious. The choice of the best value is left as the subject for future study. Below ϵ is treated as a free parameter, and the effect of its variation on the cross section will be examined and considered as part of the uncertainty due to hadronization.

Other sources of uncertainty include such technical details as how exactly the four vector of the D^* is formed. One may scale the entire four vector by z, but then the hadron mass is zm_c. Another possibility is to scale the three vector by z and fix the energy component such that that the mass is $m(D^*) = 2.01\,\mathrm{GeV}$. The latter is used here.

Evolution of the fragmentation function, which one expects to become important when $p_t \gg m_c$, is not included because the region of interest is $p_t \sim m_c$. Indeed, recent calculations of charm photoproduction at HERA [35] have shown that this effect becomes sizeable only for $p_t > 20\,\mathrm{GeV}$.

III. RESULTS

Using the results of the method described in the previous section, a computer program has been constructed to calculate charm quark and/or D^* cross sections in deeply inelastic

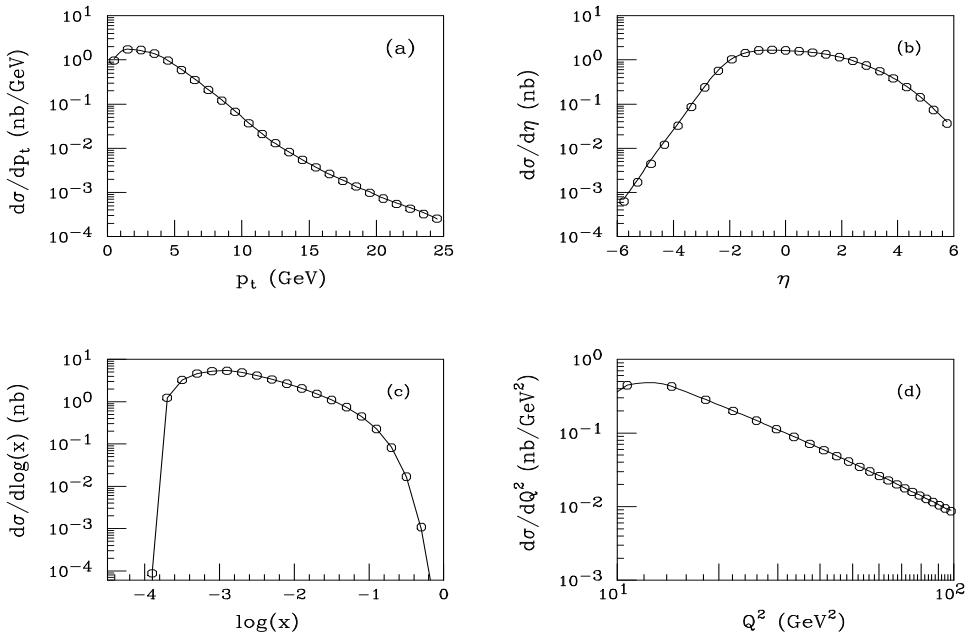

FIG. 3. Comparison of leading order results (open circles) with AROMA [36] (solid lines) for charm production in the kinematic region $10 < Q^2 < 100\,\mathrm{GeV}^2$ and $0 < y < 0.7$ at HERA.

scattering [1]. The program uses Monte Carlo integration so it is possible to study a variety of distributions and implement experimental cuts, provided they are defined in terms of partonic variables or the optional fragmentation into heavy hadrons is used. Results are presented in the HERA lab frame with positive rapidity in the proton direction. The proton and electron beam energies are taken to be 820 GeV and 27.6 GeV, respectively. There are several necessary cross checks that should be performed before discussing the general properties of the complete next-to-leading order calculation.

A. Comparison with existing results

A comparison with the leading order event generator AROMA [36] provides a check on the kinematics and leading order matrix elements through the shape and overall normalization of the distributions. For this purpose, both codes were run with the CTEQ2L [37] proton parton distributions, the default set for AROMA. This set has $\Lambda^{(4)} = 190\,\mathrm{MeV}$ which was used, along with $n_f = 4$, in the one-loop strong coupling α_s. The renormalization and factorization scales were both set to $\sqrt{\hat{s}}$. In the AROMA calling program all fragmentation and showering was turned off, and only the contribution from virtual photon exchange was retained. Shown in FIG. 3 are the results for charm quark production, assuming $m_c = 1.5\,\mathrm{GeV}$, in the kinematic region $10 < Q^2 < 100\,\mathrm{GeV}^2$ and $0 < y < 0.7$. The distributions shown are for the transverse momentum p_t and pseudo-rapidity η of the charm

[1]Interested readers should contact `harris@hep.fsu.edu` for a copy of the computer code.

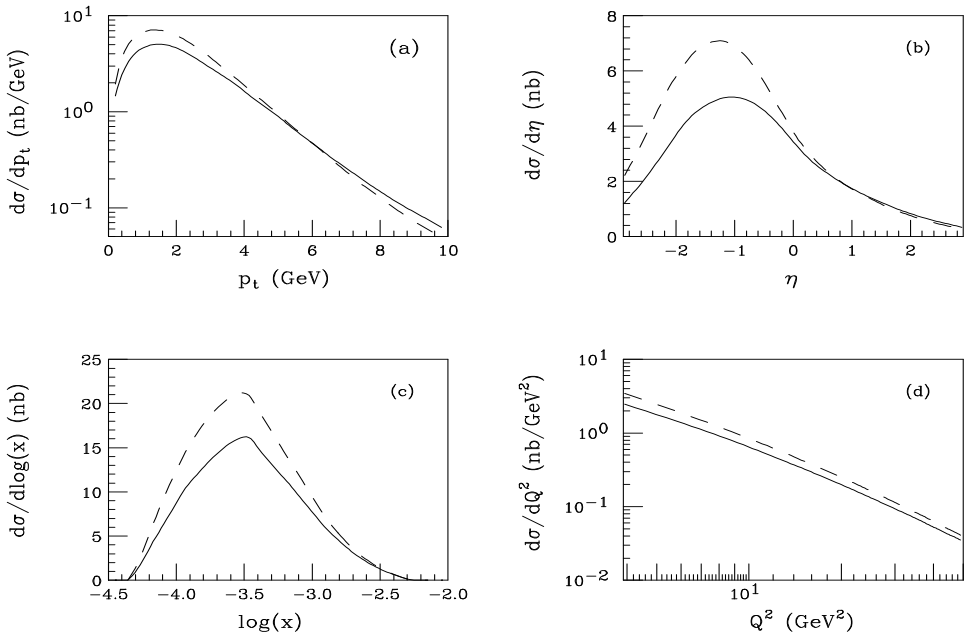

FIG. 4. Leading (dash) and full next-to-leading (solid) order differential cross sections for charm quark production at $\sqrt{S} = 301\,\mathrm{GeV}$ at HERA using the GRV94 (LO and HO, respectively) parton distribution set at $\mu = \sqrt{Q^2 + 4m_c^2}$ with $m_c = 1.5\,\mathrm{GeV}$.

quark, both in the HERA lab frame, along with the usual deep inelastic scattering variables x and Q^2. These will be the canonical set of observables used in the rest of the paper. The shapes of the curves are virtually identical over several orders of magnitude and the area under the curves is the same to better than 1%.

Another check is to reproduce the total heavy quark cross section as previously calculated in next-to-leading order [25]. Both computer programs were run with the CTEQ3M [37] proton parton distributions. This set has $\Lambda^{(4)} = 239\,\mathrm{MeV}$ which was used, along with $n_f = 4$, in the two-loop strong coupling α_s. The renormalization and factorization scales were both set to $\sqrt{Q^2 + 4m_c^2}$. The results for charm quark production, again assuming $m_c = 1.5\,\mathrm{GeV}$, in the kinematic region $10 < Q^2 < 100\,\mathrm{GeV}^2$ and $0.01 < y < 0.7$ are identical for both programs to better than three significant figures. The numerical values for the cross section per channel are 7.48 nb for $\mathcal{O}(\alpha_s)$ photon-gluon, 2.68 nb for $\mathcal{O}(\alpha_s^2)$ photon-gluon, and -0.41 nb for the sum of photon-quark and photon-antiquark. Having made these checks, the general properties of the full next-to-leading order cross section may now be considered.

B. Properties of the charm quark cross section

In this section the dependence of the charm quark cross sections will be studied as a function of parton distribution set, charm quark mass, and renormalization/factorization scale. All results are for the kinematic range $3 < Q^2 < 50\,\mathrm{GeV}^2$ and $0.1 < y < 0.7$.

The CTEQ4F3 [38] and GRV94 HO [23] proton-parton distribution sets were used in the remainder of the paper, as noted. For leading order results, the GRV94 LO [23] set

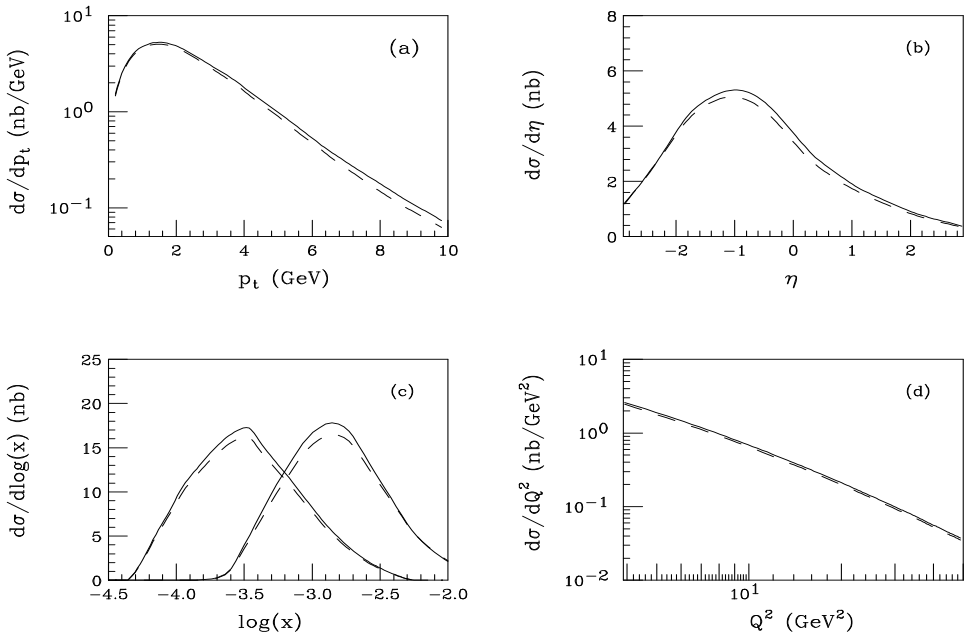

FIG. 5. Next-to-leading order differential cross sections for charm quark production at $\sqrt{S} = 301\,\mathrm{GeV}$ at HERA using the GRV94 (dash) and CTEQ4F3 (solid) parton distribution sets at $\mu = \sqrt{Q^2 + 4m_c^2}$ with $m_c = 1.5\,\mathrm{GeV}$. Also shown for comparison in part (c) is $d\sigma/d\log(\xi)$ vs. $\log(\xi)$ (right pair of curves).

was used. The (one-) two-loop version of the strong coupling α_s was used with matching across quark thresholds for the (LO) NLO results. The value of Λ_{QCD} was taken from the proton-parton distribution set. The renormalization and factorization scales have been set equal to μ.

The leading (dash) and next-to-leading (solid) order differential cross sections for charm quark production using the GRV94 (LO and HO, respectively) parton distribution set at $\mu = \sqrt{Q^2 + 4m_c^2}$ with $m_c = 1.5\,\mathrm{GeV}$ are shown in FIG. 4. The shape of the NLO transverse momentum distribution is similar to the LO one, but somewhat flatter. The pseudo-rapidity distribution shows the radiative corrections are concentrated in the negative rapidity direction, tending to pull the maximum back towards the central region. The Bjorken x distribution receives corrections near its maximum with near zero correction at the tails. The Q^2 distribution receives a fairly uniform shift in normalization. Save at high p_t, the NLO predictions lie below the LO ones. This a property of the GRV parton distribution set. For the CTEQ4F3 set the opposite behavior is observed. This a reflection of the difference between the leading order gluon distribution functions and the corresponding Λ_{QCD} of the two sets.

One may ask how sensitive are the full next-to-leading order results to modern parton distribution sets. The answer is immediate from FIG. 5 which shows the next-to-leading order differential cross sections for charm quark production using the GRV94 (dash) and CTEQ4F3 (solid) parton distribution sets at $\mu = \sqrt{Q^2 + 4m_c^2}$ with $m_c = 1.5\,\mathrm{GeV}$. From Eq. (2.7) the parton distributions are probed at ξ which is typically one order of magnitude larger the x. This is illustrated in FIG. 5c where a plot of $d\sigma/d\log(\xi)$ vs. $\log(\xi)$ (right set of curves)

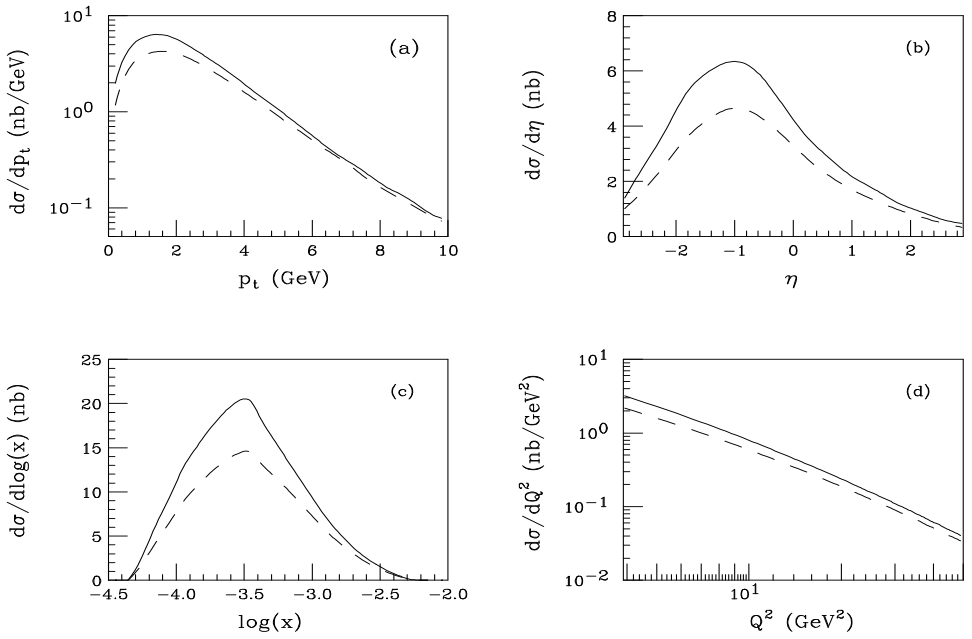

FIG. 6. Next-to-leading order differential cross sections for charm quark production at $\sqrt{S} = 301\,\mathrm{GeV}$ at HERA using the CTEQ4F3 parton distribution set at $\mu = \sqrt{Q^2 + 4m_c^2}$ with $m_c = 1.35\,\mathrm{GeV}$ (solid) and $m_c = 1.65\,\mathrm{GeV}$ (dash).

is superimposed on the plot of $d\sigma/d\log(x)$ vs. $\log(x)$ (left set of curves). The difference between the curves produced using the two parton distribution sets is approximately 10% at $\xi = 10^{-2.7}$. Thus, the predictions are less dependent on the parton density sets in NLO.

The largest uncertainty in the structure function calculation is that of the charm quark mass. The same is true for the cross section as shown in FIG. 6 for the next-to-leading order differential cross sections for charm quark production using the CTEQ4F3 parton distribution set at $\mu = \sqrt{Q^2 + 4m_c^2}$ with $m_c = 1.35\,\mathrm{GeV}$ (solid) and $m_c = 1.65\,\mathrm{GeV}$ (dash). Mass effects are smaller at the larger transverse mass because they are suppressed by powers of m_c/p_t in the matrix elements. However, as mentioned above, if the range is extended much further, large logarithms of the form $\ln(p_t^2/m_c^2)$ appear in the cross section and should be resummed.

Finally, the scale dependence is shown in FIG. 7. The next-to-leading order differential cross sections are for the CTEQ4F3 parton distribution set at $\mu = 2m_c$ (solid) and $\mu = 2\sqrt{Q^2 + 4m_c^2}$ (dash) with $m_c = 1.5\,\mathrm{GeV}$. The curves show very little scale dependence. This can be anticipated from the results shown in FIG. 2 and the distribution in Bjorken x shown in FIG. 7c. The latter shows the cross section is dominated by $x \sim 10^{-3.5} = 3.2 \times 10^{-4}$ while the former shows that, independent of Q^2, the structure function is very flat in this particular x region. Therefore, the cross section tends to be fairly insensitive to the choice of scale. Other kinematic regions show increased scale dependence. This serves as a reminder that care must be taken in interpreting the results of varying the renormalization/factorization scale to estimate the size of the theoretical error.

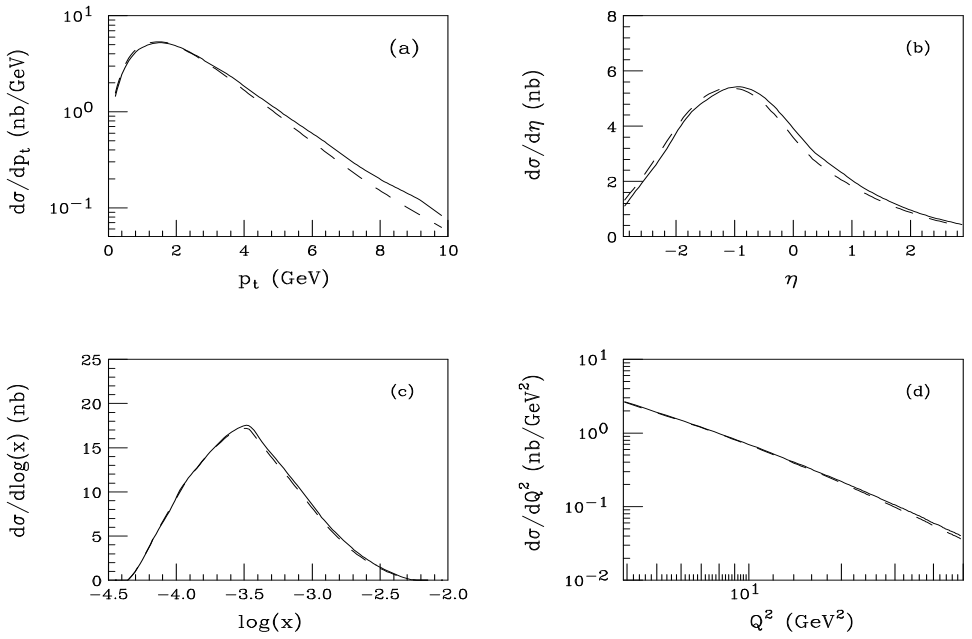

FIG. 7. Next-to-leading order differential cross sections for charm quark production at $\sqrt{S} = 301\,\mathrm{GeV}$ at HERA using the CTEQ4F3 parton distribution set at $\mu = 2m_c$ (solid) and $\mu = 2\sqrt{Q^2 + 4m_c^2}$ (dash) with $m_c = 1.5\,\mathrm{GeV}$.

C. Predictions for D^* production

In this last section the fragmentation is turned on and predictions for $D^{*\pm}$ production at HERA are given. The power of the subtraction method becomes manifest because experimental cuts can easily be implemented. Cuts similar to those preferred by ZEUS [1] and H1 [2] are used. Namely, $2 < Q^2 < 100\,\mathrm{GeV}^2$, $0.05 < y < 0.7$, $p_t^{D^*} > 1.5\,\mathrm{GeV}$, and $|\eta^{D^*}| < 1.5$. No distinction is made between D^{*+} and D^{*-}. The results shown in FIG. 8 use the GRV94 parton distribution set at $\mu = \sqrt{Q^2 + 4m_c^2}$ with $m_c = 1.5\,\mathrm{GeV}$ and $\epsilon = 0.03$ (dot), $\epsilon = 0.06$ (solid), $\epsilon = 0.09$ (dash). The variation in the area under the curves is roughly half that from the mass uncertainty. The shape changes are very mild. Using the CTEQ4F3 parton distribution set instead would give slightly larger results.

IV. CONCLUSION

The calculation of next-to-leading order corrections has allowed more reliable predictions of heavy quark differential distributions in deeply inelastic scattering. In addition, with the calculational formalism used here, it was possible to add Peterson fragmentation thus giving predictions for $D^{*\pm}(2010)$ production at HERA.

At leading order the results were cross checked against AROMA and found to give complete agreement. When the program is run in fully inclusive mode it reproduces existing results for the charm quark cross section at next-to-leading order.

The radiative corrections to the lowest order photon-gluon fusion process are important

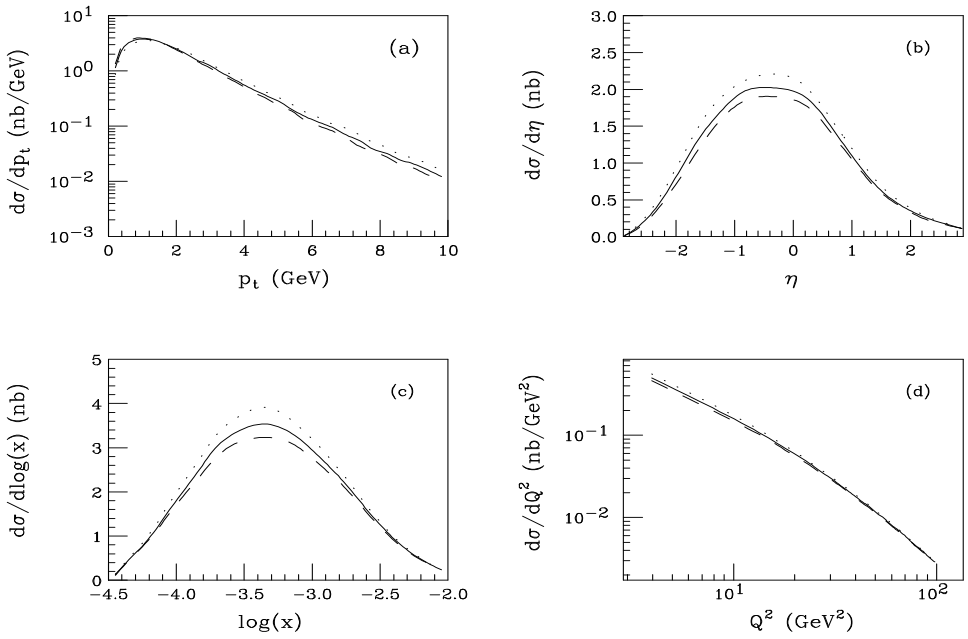

FIG. 8. Next-to-leading order differential cross sections for D^* production at $\sqrt{S} = 301\,\mathrm{GeV}$ at HERA in the kinematic region $0.05 < y < 0.7$, $2 < Q^2 < 100\,\mathrm{GeV}^2$, $1.5 < P_t^{D^*} < 10\,\mathrm{GeV}$, and $|\eta^{D^*}| < 1.5$ using the GRV94 parton distribution set at $\mu = \sqrt{Q^2 + 4m_c^2}$ with $m_c = 1.5\,\mathrm{GeV}$ and $\epsilon = 0.03$ (dot), $\epsilon = 0.06$ (solid), $\epsilon = 0.09$ (dash).

as they change both the shape and normalization of the transverse momentum, pseudo-rapidity, and x distributions. The Q^2 distributions only receive a shift in normalization. In the kinematic region studied, the cross section is very stable with respect to variations in the renormalization/factorization scale because the cross section is dominated by an x region where the scale dependence of the underlying structure functions is nearly flat. The scale dependence of the hard scattering cross sections is well compensated by that of the parton densities and α_s.

The cross section is dominated by the rapidly growing gluon distribution at small x, but distinguishing between modern parton distribution sets using this process will be difficult as demonstrated by the fact that they give nearly identical results for a variety of observables. This is compounded by relatively large uncertainties from the quark mass and hadronization effects. At present a comparison with experimental data can offer a confirmation of the gluon distribution at small x. Examining a variety of x and Q^2 bins will shed light on the transition region between massive and massless charm quark descriptions.

ACKNOWLEDGMENTS

This work was support by contracts DE-FG02-97ER41022 and NSF 93-09888. We thank J.F. Owens for comments, J.P. Fernández for discussions concerning the ZEUS analysis, and F. Sefkow and K. Daum for discussions concerning the H1 analysis. J. Smith would like to thank the Alexander von Humbolt Foundation for an award allowing him to spend his

sabbatical leave at DESY.

REFERENCES

[1] M. Derrick *et al.* (ZEUS Collab.), *Phys. Lett.* B **349**, 225 (1995); M. Derrick *et al.* (ZEUS Collab.), *XXVIII Int. Conf. on HEP '96*, Warsaw (1996); J. Breitweg *et al.* (ZEUS Collab.), *Phys. Lett.* B **407**, 402 (1997).

[2] C. Adloff *et al.* (H1 Collab.), *Z. Phys.* C **72**, 593 (1996).

[3] E. Laenen, S. Riemersma, J. Smith, and W.L. van Neerven, *Nucl. Phys.* B **392**, 162 (1993).

[4] E. Laenen, S. Riemersma, J. Smith, and W.L. van Neerven, *Nucl. Phys.* B **392**, 229 (1993).

[5] B.W. Harris and J. Smith, *Nucl. Phys.* B **452**, 109 (1995).

[6] J.J. Aubert *et al.* (EMC Collab.), *Nucl. Phys.* B **213**, 31 (1983); see also B.W. Harris, J. Smith and R. Vogt, *Nucl. Phys.* B **461**, 181 (1996).

[7] F.I. Olness and S. Riemersma, *Phys. Rev.* D **51**, 4746 (1995).

[8] M. Glück, E. Reya, and M. Stratmann, *Nucl. Phys.* B **422**, 37 (1994).

[9] M.A.G. Aivazis, J.C. Collins, F.I. Olness, and W.K. Tung, *Phys. Rev.* D **50**, 3102 (1994).

[10] A.D. Martin, R.G. Roberts, M.G. Ryskin and W.J. Stirling, DPT-96-102, [hep-ph/9612449].

[11] M. Buza, Y. Matiounine, J. Smith and W.L. van Neerven, DESY 96-258, [hep-ph/9612398]; DESY 97-124 [hep-ph/9707263]; *Phys. Lett.* B **411**, 211 (1997).

[12] B.W. Harris, in *Minneapolis Meeting of the Division of Particles and Fields of the American Physical Society*, Minneapolis, 1996, editied by J.K. Nelson and K. Heller (World Scientific, Singapore, 1996).

[13] M. Mangano, P. Nason, and G. Ridolfi, *Nucl. Phys.* B **373**, 295 (1992). For a leading order discussion see, for example, E. Berger, *Phys. Rev.* D **37**, 1810 (1988).

[14] S. Frixione, M. Mangano, P. Nason, and G. Ridolfi, *Nucl. Phys.* B **412**, 225 (1994).

[15] M. Krämer and E. Laenen, *Phys. Lett.* B **371**, 303 (1996).

[16] B.W. Harris and J.F. Owens, *Phys. Rev.* D **54**, 2295 (1996).

[17] R.K. Ellis, D.A. Ross, and A.E. Terrano, *Nucl. Phys.* B **178**, 421 (1981).

[18] L.J. Bergmann, Ph.D. thesis, Florida State University, 1989; H. Baer, J. Ohnemus, and J.F. Owens, *Phys. Rev.* D **40**, 2284 (1989); W. T. Giele and E.W.N. Glover, *Phys. Rev.* D **46**, 1980 (1992).

[19] Z. Kunszt and D.E. Soper, *Phys. Rev.* D **46**, 192 (1992).

[20] G.A. Schuler, *Nucl. Phys.* B **299**, 21 (1988).

[21] J.C. Collins, F. Wilczek and A. Zee, *Phys. Rev.* D **18**, 42 (1978); J.C. Collins and W.K. Tung, *Nucl. Phys.* B **278**, 934 (1986).

[22] P. Nason, S. Dawson, and R.K. Ellis, *Nucl. Phys.* B **327**, 49 (1989).

[23] M. Glück, E. Reya and A. Vogt, *Z. Phys.* C **67**, 433 (1995).

[24] H.L. Lai and W.K. Tung, *Z. Phys.* C **74**, 463 (1997).

[25] S. Riemersma, J. Smith, and W.L. van Neerven, *Phys. Lett.* B **347**, 143 (1995).

[26] M. Buza, Y. Matiounine, J. Smith, R. Migneron and W.L. van Neerven, *Nucl. Phys.* B **472**, 611 (1996).

[27] A. Vogt, in *International Workshop on Deep Inelastic Scattering and Related Phenomena (DIS 96)*, Rome, 1996, edited by G. D'Agostini and A. Nigro (World Scientific, Singapore, 1997), p. 254.

[28] K. Daum, S. Riemersma, B.W. Harris, E. Laenen, and J. Smith in *Proceedings of the Workshop 1995/96 on Future Physics at HERA, Hamburg, 1996*, edited by G. Ingelman et al. (Deutches Elektronen-Synchrotron, Hamburg, 1996), p. 89.
[29] E. Laenen, M. Buza, B.W. Harris, Y. Matiounine, R. Migneron, S. Riemersma, J. Smith, and W.L. van Neerven in *Proceedings of the Workshop 1995/96 on Future Physics at HERA, Hamburg, 1996*, edited by G. Ingelman et al. (Deutches Elektronen-Synchrotron, Hamburg, 1996), p. 393.
[30] C. Peterson, D. Schlatter, I. Schmitt, and P.M. Zerwas, *Phys. Rev.* D **27**, 105 (1983).
[31] R. Akers *et al.* (OPAL Collab.), *Z. Phys.* C **67**, 27 (1995).
[32] J. Chrin, *Z. Phys.* C **36**, 163 (1987).
[33] M. Cacciari and M. Greco, *Phys. Rev.* D **55**, 7134 (1997)
[34] J. Binnewies, B.A. Kniehl, and G. Kramer, DESY 97-012, [hep-ph/9702408].
[35] M. Cacciari and M. Greco, *Z. Phys.* C **69**, 459 (1996); B.A. Kniehl, M. Krämer, G. Kramer, and M. Spira, *Phys. Lett.* B **356**, 539 (1995).
[36] G. Ingelman, J. Rathsman, and G.A. Schuler, *Comput. Phys. Commun.* **101**, 135 (1997).
[37] H.L. Lai, J. Botts, J. Huston, J.G. Morfin, J.F. Owens, J.W. Qiu, W.K. Tung, and H. Weerts, *Phys. Rev.* D **51**, 4763 (1995).
[38] H.L. Lai, J. Huston, S. Kuhlmann, F. Olness, J.F. Owens, D. Soper, W.K. Tung, and H. Weerts, *Phys. Rev.* D **55**, 1280 (1997);